The Astrophysical Journal, 706:1588–1593, 2009 December 1 doi:10.1088/0004-637X/706/2/1588

LABORATORY DETECTION OF THIOCYANIC ACID HSCN

S. Brünken[1,2,3], Z. Yu[1,2,4], C. A. Gottlieb[1,2], M. C. McCarthy[1,2], and P. Thaddeus[1,2]
[1] Harvard-Smithsonian Center for Astrophysics, 60 Garden St., Cambridge, MA 02138, USA
[2] School of Engineering & Applied Sciences, Harvard University, 29 Oxford St., Cambridge, MA 02138, USA; sbruenken@cfa.harvard.edu, cgottlieb@cfa.harvard.edu, mccarthy@cfa.harvard.edu, pthaddeus@cfa.harvard.edu
Received 2009 May 18; accepted 2009 October 8; published 2009 November 16

ABSTRACT

The rotational spectrum of thiocyanic acid HSCN, a highly polar isomer of the well-known astronomical molecule isothiocyanic acid HNCS, has been measured in two radio bands: in the centimeter-wave band by Fourier transform microwave spectroscopy in a molecular beam, and in the millimeter-wave band by long-path absorption spectroscopy in a low-pressure glow discharge. Twelve spectroscopic constants were derived from more than 60 a-type rotational transitions between 11 and 346 GHz with J up to 30 and $K_a \leqslant 6$, including seven centimeter-wave transitions with resolved hyperfine structure. With these constants the rotational spectrum in the $K_a = 0$ and $K_a = 1$ ladders—those most likely to be observed in space—can now be calculated up to 400 GHz with formal uncertainties of less than 0.2 km s^{-1} in equivalent radial velocity. Thiocyanic acid was recently identified in Sgr B2 by Halfen et al. following the laboratory measurements, and there is possible evidence for it in cold dark clouds, with the implication that HSCN may be detectable in many galactic sources.

Key words: ISM: individual (Sgr B2) – ISM: molecules – line: identification – molecular data – molecular processes – radio lines: ISM

1. INTRODUCTION

Isothiocyanic acid HNCS, long known as a constituent of the interstellar medium, was detected 30 years ago via several a-type $K_a = 0$ rotational transitions in Sgr B2 (Frerking et al. 1979). Like isovalent HNCO, HNCS is calculated to be the most stable molecule with its elemental composition, and to possess a singlet ground state with a nearly linear heavy atom backbone and a planar equilibrium structure. The rotational spectrum of HNCS was first measured nearly 50 years ago by Beard & Dailey (1950); since then it has been the subject of many high-resolution studies, from the microwave band to the far infrared (Kewley et al. 1963; Yamada et al. 1979, 1980; Rodler et al. 1987; Niedenhoff et al. 1997). Much of this work aimed at understanding the influence of large-amplitude bending vibrations on structural rigidity.

Although the derived abundance of HNCS relative to HNCO in Sgr B2 is consistent with the cosmic S/O ratio of 1/42 (Frerking et al. 1979), other small sulfur-bearing molecules (e.g., CCS: Saito et al. 1987; C_3S: Yamamoto et al. 1987, etc.) were subsequently found in space with abundances greater than their oxygen counterparts. Despite extensive astronomical observations and chemical modeling of these molecules (Hatchell et al. 1998), sulfur chemistry is still not well understood, largely because the major reservoir of sulfur in dense molecular clouds has not been established (see Wakelam et al. 2004). In light of recent work, the close agreement between the HNCS/HNCO and cosmic S/O ratios may be fortuitous. The recent astronomical detection of two high-lying CHNO isomers—HOCN (Brünken et al. 2009a, 2009b), calculated to lie 25 kcal mol^{-1} higher in energy than HNCO, and HCNO (Marcelino et al. 2009), a surprising 71 kcal mol^{-1} higher in energy (Schuurman et al. 2004)—illustrates that current chemical models poorly predict the formation of the energetic isomers in these two related families of molecules.

Thiocyanic acid HSCN is calculated to be the second most stable isomer of isothiocyanic acid, lying 4–14 kcal mol^{-1} (0.2–0.6 eV) above HNCS (Wierzejewska & Moc 2003; Durig et al. 2006), the precise energy difference depending on the level of theory and the basis set adopted in the quantum calculations. The a-component of the dipole moment of HSCN is also predicted to be substantial ($\mu_a = 3.46$ D)—twice that of HNCS ($\mu_a = 1.72$ D). Because HSCN is a low-lying, highly polar isomer, it was desirable to precisely measure its rotational spectrum so that a radioastronomical search could be undertaken. To date, HSCN had only been characterized experimentally at low spectral resolution by matrix-IR spectroscopy, where it was formed by UV-photolysis of HNCS in solid argon and nitrogen (Wierzejewska & Mielke 2001). In the original study of the rotational spectrum of HNCS, Beard & Dailey (1950) were unable to detect any evidence for HSCN, concluding that "thiocyanic acid" in its vapor state consists of at least 95% HNCS. The only two unidentified lines in their observed spectrum we now know arise from rotational transitions in the low-lying v_6 vibrationally excited state of HNCS (Kewley et al. 1963).

Here we report the first gas-phase measurements of HSCN, and a precise determination of its rotational spectrum by Fourier transform microwave (FTM) spectroscopy between 10 and 35 GHz, and free space millimeter-wave absorption spectroscopy between 75 and 350 GHz. From the derived spectroscopic constants, the astronomically most interesting radio lines of this polar isomer of HNCS up to 400 GHz can be predicted with formal uncertainties of less than 0.2 km s^{-1} in equivalent radial velocity.

2. LABORATORY MEASUREMENTS AND RESULTS

Thiocyanic acid is a closed-shell asymmetric rotor very close to the prolate limit ($\kappa = -0.99919$), with the a principal axis of inertia closely coincident with the nearly linear heavy

[3] Current address: I. Physikalisches Institut, Universität zu Köln, Zülpicher Str. 77, 50937 Köln, Germany.
[4] Current address: Aerodyne Research, Inc., 45 Manning Road, Billerica, MA 01821, USA.

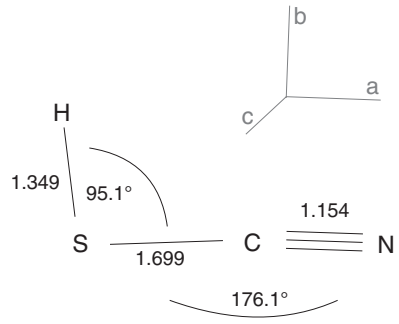

Figure 1. Equilibrium structure of thiocyanic acid calculated at the B3LYP/aug-cc-pVTZ level of theory (Wierzejewska & Moc 2003). Bond lengths are in Å and angles in degrees.

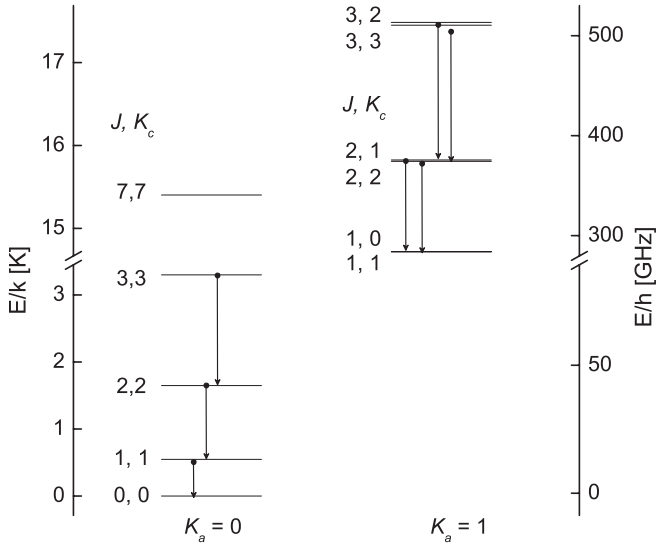

Figure 2. Energy level diagram of the lowest rotational levels of HSCN. Transitions measured by FTM spectroscopy are indicated by arrows.

atom backbone (see Figure 1). For this reason, it has a large A rotational constant and a large separation between successive K_a levels (∼15 K), as the energy level diagram in Figure 2 shows. The a-type spectrum of HSCN is expected to be significantly more intense than the b-type spectrum, owing to the large difference in dipole moments along the two principal inertial axes ($\mu_a = 3.46$ D versus $\mu_b = 1.09$ D).

The present apparatus has been described in detail previously (McCarthy et al. 2000; Gottlieb et al. 2003). In the centimeter-wave band, HSCN was produced in the throat of a pulsed supersonic discharge nozzle. As the discharge products expand from the nozzle into the confocal Fabry–Perot cavity, they undergo rapid adiabatic cooling; near the center of the cavity, the effective rotational temperature may be as low as 1 K. The gas mixture consisted of either acetonitrile (CH_3CN, 0.2%) or cyanogen ($(CN)_2$, 0.2%), and hydrogen sulfide (H_2S, 0.2%) diluted in an inert buffer gas (Ne). The strongest lines were obtained with a discharge potential of 900 V and a gas pulse duration of ∼300 μs. In the millimeter-wave band, HSCN was produced in a low-pressure dc discharge through hydrogen sulfide and cyanogen in a 2:1 mixture in Ar. The total pressure in our free space absorption cell was about 20 mtorr with the walls of the cell cooled to approximately 200 K. A discharge current of 100 mA was found to optimize transitions of both HNCS and HSCN, with the lines of HNCS approximately three times more intense than those of HSCN.

Table 1
Centimeter-wave Laboratory Frequencies of HSCN

Transition		Frequency	$O-C$[a]
$J'_{K'_a,K'_c}$–J_{K_a,K_c}	$F'-F$	(MHz)	(kHz)
$1_{0,1}$–$0_{0,0}$	1–1	11468.633(2)	−1
	2–1	11469.851(2)	2
	0–1	11471.669(2)	−1
$2_{1,2}$–$1_{1,1}$	2–1	22817.864(2)	3
	1–1	22818.474(2)	3
	2–2	22818.711(2)	2
	3–2	22819.107(2)	6
	1–0	22820.591(2)	−1
$2_{0,2}$–$1_{0,1}$	2–2	22937.998(2)	−3
	1–0	22938.201(2)	−2
	2–1	22939.214(2)	−1
	3–2	22939.302(2)	1
	1–1	22941.237(2)	−2
$2_{1,1}$–$1_{1,0}$	2–1	23057.406(2)	−1
	3–2	23058.688(2)	6
	2–2	23057.769(2)	−4
	1–0	23059.735(2)	−1
	1–1	23058.819(2)	−2
$3_{1,3}$–$2_{1,2}$	3–3	34227.537(2)	−6
	3–2	34227.938(2)	3
	4–3	34228.291(2)	4
	2–1	34228.326(2)	−3
	2–2	34228.936(2)	−4
$3_{0,3}$–$2_{0,2}$	3–3	34407.326(2)	−1
	2–1	34408.424(2)	−1
	3–2	34408.629(2)	1
	4–3	34408.678(2)	2
	2–2	34410.447(2)	−2
$3_{1,2}$–$2_{1,1}$	3–3	34586.340(2)	−1
	3–2	34587.252(2)	2
	2–1	34587.564(2)	0
	4–3	34587.625(2)	4
	2–2	34588.978(2)	0

Notes. Three strongest ($\Delta F = 1$) hyperfine components of the $J = 4 \rightarrow 3$ transition calculated from the full set of constants in Table 3: $4_{1,4} \rightarrow 3_{1,3}$: 45637.256 ($4 \rightarrow 3$), 45637.382 ($3 \rightarrow 2$), 45637.411 ($5 \rightarrow 4$); $4_{0,3} \rightarrow 3_{0,2}$: 45877.720 ($3 \rightarrow 2$), 45877.807 ($4 \rightarrow 3$), 45877.838 ($5 \rightarrow 4$); $4_{1,3} \rightarrow 3_{1,2}$: 46116.335 ($4 \rightarrow 3$), 46116.426 ($3 \rightarrow 2$), 46116.502 ($5 \rightarrow 4$). The 1$\sigma$ uncertainties in the calculated frequencies are ±0.001 MHz.
[a] Calculated from the spectroscopic constants in Table 3.

2.1. Centimeter-wave Spectrum

Our laboratory search for HSCN was guided by rotational constants derived from published quantum calculations (Wierzejewska & Moc 2003; Durig et al. 2006), and nitrogen-14 quadrupole coupling constants calculated by us. A search near 11.5 GHz, the predicted frequency of the fundamental a-type rotational transition ($J_{K_a,K_c} = 1_{0,1} \rightarrow 0_{0,0}$), was undertaken first. A triplet pattern, with the expected line spacing and relative intensities characteristic of the expected hyperfine structure (hfs) was found within 5 MHz of the prediction. Two other lines closely harmonic in frequency, the $2_{0,2} \rightarrow 1_{0,1}$ and $3_{0,3} \rightarrow 2_{0,2}$ transitions, were then found, as were lines in the $K_a = 1$ ladder which were within 25 MHz of the predictions. As the arrows in Figure 2 show, seven a-type transitions, three in the $K_a = 0$ ladder, and four in $K_a = 1$, were detected in the centimeter-wave band (Table 1). Owing to the low rotational temperature of the supersonic beam, the intensity of the $K_a = 1$ lines was a factor of 1000 less than that in the $K_a = 0$ ladder, so no

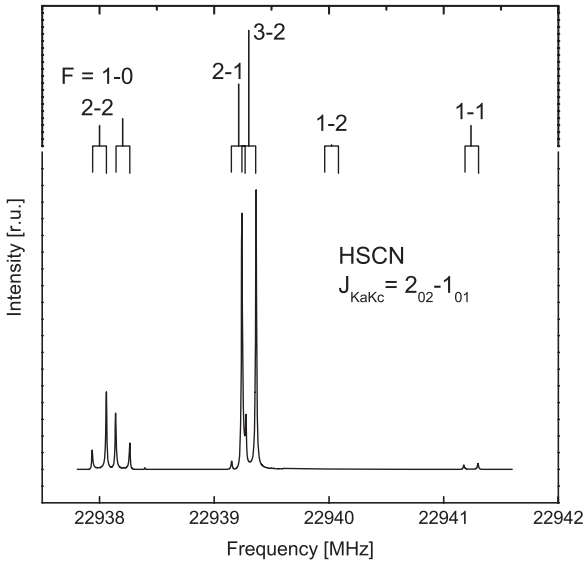

Figure 3. Calculated (top) and observed (bottom) spectra of the $J_{K_a,K_c} = 2_{0,2}$–$1_{0,1}$ transition of HSCN with resolved nitrogen hyperfine structure. Each line is split into two components, owing to the interaction of the supersonic molecular beam with the standing wave in the confocal Fabry–Perot cavity of the spectrometer.

attempt was made to search for higher K_a transitions with our FTM spectrometer.

There is very little doubt that all of the assigned lines are from HSCN, and no other molecule. The close harmonicity of lines in the $K_a = 0$ ladder and the absence of fine structure confirms that the carrier is a closed-shell molecule. The measured rotational constants B and C agree to better than 0.2% with those predicted from two theoretical calculations (Wierzejewska & Moc 2003; Durig et al. 2006), providing strong evidence that HSCN is the carrier of the observed lines. Hfs in the lower rotational transitions and quadrupole coupling constants within 15% of those predicted show that the molecule contains nitrogen, as illustrated in the sample spectrum of the $2_{0,2} - 1_{0,1}$ transition (Figure 3). Conclusive confirmation of our assignment was provided by detection of DSCN with an isotope shift of 2.40%, that is within 0.01% of that predicted, as well as well resolved deuterium and nitrogen-14 hfs in the centimeter-wave rotational lines.

2.2. *Millimeter-wave Spectrum*

From a preliminary set of rotational constants derived from the FTM measurements, transitions in the $K_a = 0$ and 1 ladders were observed with our free space millimeter-wave spectrometer. Many strong background lines were present in our discharge, but those of HSCN in the two lowest ladders were readily identified, because they were within 5 MHz of the predicted positions. Refinement of the spectroscopic constants following the identification of lines with successively higher K_a, allowed precise measurements of transitions with K_a up to 6 (see Figure 4 for a sample spectrum of an R-branch series near 172 GHz). Summarized in Table 2 are the measured millimeter-wave frequencies.

In all, more than 60 rotational transitions with J up to 30 and $K_a \leqslant 6$, including seven in the centimeter-wave band with resolved hfs, were analyzed with Watson's S-reduced Hamiltonian. The experimental frequencies were reproduced to within the measurement uncertainties with three rotational constants, seven centrifugal distortion constants including one

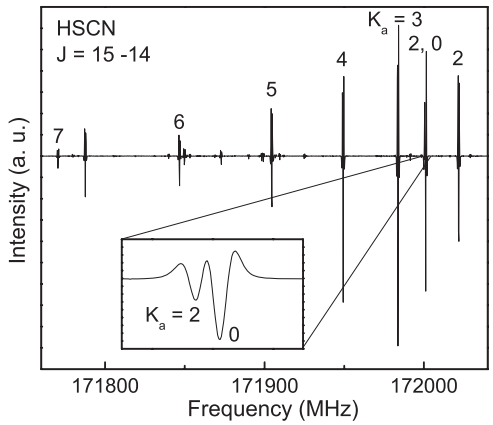

Figure 4. R-branch $K_a = 0, 2$–7 spectrum of the $J = 15$–14 transition of HSCN. The inset shows the $15_{0,15}$–$14_{0,14}$ and $15_{2,14}$–$14_{2,13}$ lines observed with higher frequency resolution and signal to noise on an expanded frequency scale. The instrumental line shape is approximately the second derivative of a Lorentzian profile, owing to the detection scheme employed.

eighth-order constant, and two quadrupole coupling constants. Adding a second eighth-order distortion constant (L_{KJ}) reduced the rms (28 kHz) only slightly, so L_{KJ} was constrained to zero. The A rotational constant was not well determined because we did not observe any b-type transitions. Owing to the high correlation with the K_a dependent centrifugal distortion constants (D_K, H_K, and L_K) and the very weak dependence of the R-branch ($\Delta J = 1, \Delta K_a = 0$) transitions on A, the actual uncertainty in A may be greater than the statistical uncertainty obtained with the truncated Hamiltonian.[5] Summarized in Table 3 are the measured and theoretical spectroscopic constants of HSCN and DSCN.

An accurate determination of A awaits the detection of b-type transitions, such as $1_{1,1} \rightarrow 0_{0,0}$ near 300 GHz. Although μ_b^2 is 10 times smaller than μ_a^2, transitions such as these at high frequencies will be fairly intense. The difficulty in identifying b-type transitions in the present experiment was not signal to noise, but rather resulted from: (1) uncertainties in the frequency predictions; (2) lack of harmonicity of the b-type transitions; and (3) high density of background lines in our discharge source.

The rotational spectrum of HSCN in the $K_a = 0$ and 1 ladders (those mainly expected to be populated in the interstellar gas) can now be predicted with formal uncertainties of better than 0.2 km s^{-1} in equivalent radial velocity up to 400 GHz with the constants in Table 4. The spectroscopic constants in Table 3 might not be sufficiently accurate to predict frequencies of lines with higher K_a, because HSCN like HNCS (Niedenhoff et al. 1995) is expected to show effects of quasi-linearity characterized by large centrifugal distortion[6] and slow convergence of the effective rotational Hamiltonian, particularly for purely K_a dependent terms. Measurements of lines in higher K_a ladders confirm this expectation. For example, several tentatively assigned lines with $K_a = 7$ differ by 1–2 MHz from those predicted with the spectroscopic constants in Table 3, and the addition of still higher-order distortion fails to remove this discrepancy possibly owing to omission of the K_a dependent terms D_K and H_K in the Hamiltonian. A more extensive analysis of the rotational spectrum of HSCN is anticipated.

[5] The correlation of A with D_{JK} and H_{JK} is not very large: 0.5–0.6.

[6] Although the fourth-order distortion constants of HSCN are comparable to those of SO_2 (Müller & Brünken 2005), H_{KJ} and H_{JK} are roughly 10 times, and L_{KKJ} is 1000 times greater in HSCN.

Table 2
Millimeter-wave Laboratory Frequencies of HSCN

Transition $J'_{K'a,K'c}(F')-J_{Ka,Kc}(F)$	Frequency[a] (MHz)	$O-C$[b] (kHz)	Transition $J'_{K'a,K'c}(F')-J_{Ka,Kc}(F)$	Frequency[a] (MHz)	$O-C$[b] (kHz)
$7_{1,7}$ (7)–$6_{1,6}$ (6)	79863.510(70)	22	$20_{5,15}-19_{5,14}$	229183.907(100)	81
$7_{1,7}$ (6)–$6_{1,6}$ (5)	79863.510(70)	9	$20_{5,16}-19_{5,15}$	229183.907(100)	81
$7_{1,7}$ (8)–$6_{1,6}$ (7)	79863.510(70)	−12	$20_{4,17}-19_{4,16}$	229244.067(50)	5
$7_{4,3}$ (7)–$6_{4,2}$ (6)	80250.441(70)	54	$20_{4,16}-19_{4,15}$	229244.067(50)	5
$7_{4,4}$ (7)–$6_{4,3}$ (6)	80250.441(70)	54	$20_{0,20}-19_{0,19}$	229289.446(50)	−6
$7_{4,3}$ (8)–$6_{4,2}$ (7)	80250.791(70)	−3	$20_{3,18}$ (20)–$19_{3,17}$ (19)	229291.126(50)	117
$7_{4,4}$ (8)–$6_{4,3}$ (7)	80250.791(70)	−3	$20_{3,18}$ (19)–$19_{3,17}$ (18)	229291.126(50)	108
$7_{4,3}$ (6)–$6_{4,2}$ (5)	80250.791(70)	−67	$20_{3,18}$ (21)–$19_{3,17}$ (20)	229291.126(50)	105
$7_{4,4}$ (6)–$6_{4,3}$ (5)	80250.791(70)	−67	$20_{3,17}$ (20)–$19_{3,16}$ (19)	229291.126(50)	−75
$7_{3,5}$ (8)–$6_{3,4}$ (7)	80266.314(70)	−33	$20_{3,17}$ (19)–$19_{3,16}$ (18)	229291.126(50)	−84
$7_{3,4}$ (8)–$6_{3,3}$ (7)	80266.314(70)	−33	$20_{3,17}$ (21)–$19_{3,16}$ (20)	229291.126(50)	−87
$7_{3,5}$ (6)–$6_{3,4}$ (5)	80266.314(70)	−54	$20_{2,19}-19_{2,18}$	229307.445(50)	37
$7_{3,4}$ (6)–$6_{3,3}$ (5)	80266.314(70)	−55	$20_{2,18}-19_{2,17}$	229357.425(50)	35
$7_{2,6}$ (7)–$6_{2,5}$ (6)	80276.520(100)	119	$20_{1,19}-19_{1,18}$	230517.744(50)	23
$7_{2,6}$ (6)–$6_{2,5}$ (5)	80276.520(100)	17	$28_{1,28}-27_{1,27}$	319288.018(50)	3
$7_{2,6}$ (8)–$6_{2,5}$ (7)	80276.520(100)	8	$28_{6,22}-27_{6,21}$	320680.289(70)	0
$7_{2,5}$ (7)–$6_{2,4}$ (6)	80278.500(100)	−8	$28_{6,23}-27_{6,22}$	320680.289(70)	0
$7_{2,5}$ (6)–$6_{2,4}$ (5)	80278.500(100)	−110	$28_{5,23}-27_{5,22}$	320789.132(70)	33
$7_{2,5}$ (8)–$6_{2,4}$ (7)	80278.500(100)	−119	$28_{5,24}-27_{5,23}$	320789.132(70)	33
$7_{0,7}$ (6)–$6_{0,6}$ (5)	80283.167(100)	23	$28_{0,28}-27_{0,27}$	320866.104(50)	−9
$7_{0,7}$ (7)–$6_{0,6}$ (6)	80283.167(100)	2	$28_{4,25}-27_{4,24}$	320874.881(70)	−40
$7_{0,7}$ (8)–$6_{0,6}$ (7)	80283.167(100)	−10	$28_{4,24}-27_{4,23}$	320874.881(70)	−40
$7_{1,6}$ (7)–$6_{1,5}$ (6)	80701.834(50)	26	$28_{3,26}-27_{3,25}$	320944.094(70)	28
$7_{1,6}$ (6)–$6_{1,5}$ (5)	80701.834(50)	21	$28_{3,25}-27_{3,24}$	320945.058(70)	−44
$7_{1,6}$ (8)–$6_{1,5}$ (7)	80701.834(50)	−13	$28_{2,27}-27_{2,26}$	320947.797(70)	24
$15_{1,15}-14_{1,14}$	171114.764(70)	27	$28_{2,26}-27_{2,25}$	321084.822(70)	34
$15_{6,9}$ (15)–$14_{6,8}$ (14)	171846.683(50)	6	$28_{1,27}-27_{1,26}$	322634.357(50)	5
$15_{6,10}$ (15)–$14_{6,9}$ (14)	171846.683(50)	6	$29_{1,29}-28_{1,28}$	330677.889(50)	20
$15_{6,9}$ (16)–$14_{6,8}$ (15)	171846.683(50)	−90	$29_{6,23}-28_{6,22}$	332122.576(50)	12
$15_{6,10}$ (16)–$14_{6,9}$ (15)	171846.683(50)	−90	$29_{6,24}-28_{6,23}$	332122.576(50)	12
$15_{6,9}$ (14)–$14_{6,8}$ (13)	171846.683(50)	−93	$29_{5,25}-28_{5,24}$	332235.385(50)	27
$15_{6,10}$ (14)–$14_{6,9}$ (13)	171846.683(50)	−93	$29_{5,24}-28_{5,23}$	332235.385(50)	27
$15_{5,10}$ (15)–$14_{5,9}$ (14)	171904.568(50)	81	$29_{0,29}-28_{0,28}$	332304.265(50)	1
$15_{5,11}$ (15)–$14_{5,10}$ (14)	171904.568(50)	81	$29_{4,26}-28_{4,25}$	332324.418(50)	−56
$15_{5,10}$ (14)–$14_{5,9}$ (13)	171904.568(50)	13	$29_{4,25}-28_{4,24}$	332324.418(50)	−56
$15_{5,11}$ (14)–$14_{5,10}$ (13)	171904.568(50)	13	$29_{3,27}-28_{3,26}$	332396.525(100)	−65
$15_{5,10}$ (16)–$14_{5,9}$ (15)	171904.568(50)	13	$29_{2,28}-28_{2,27}$	332397.567(100)	69
$15_{5,11}$ (16)–$14_{5,10}$ (15)	171904.568(50)	13	$29_{2,27}-28_{2,26}$	332549.685(50)	8
$15_{4,12}-14_{4,11}$	171949.362(70)	17	$29_{1,28}-28_{1,27}$	334143.081(50)	−1
$15_{4,11}-14_{4,10}$	171949.362(70)	17	$30_{1,30}-29_{1,29}$	342066.325(50)	−7
$15_{3,13}$ (15)–$14_{3,12}$ (14)	171983.747(70)	81	$30_{6,24}-29_{6,23}$	343563.740(50)	16
$15_{3,13}$ (14)–$14_{3,12}$ (13)	171983.747(70)	59	$30_{6,25}-29_{6,24}$	343563.740(50)	16
$15_{3,13}$ (16)–$14_{3,12}$ (15)	171983.747(70)	54	$30_{5,26}-29_{5,25}$	343680.553(50)	40
$15_{3,12}$ (15)–$14_{3,11}$ (14)	171983.747(70)	36	$30_{5,25}-29_{5,24}$	343680.553(50)	40
$15_{3,12}$ (14)–$14_{3,11}$ (13)	171983.747(70)	14	$30_{0,30}-29_{0,29}$	343740.186(50)	8
$15_{3,12}$ (16)–$14_{3,11}$ (15)	171983.747(70)	9	$30_{4,27}-29_{4,26}$	343772.872(50)	−75
$15_{2,14}-14_{2,13}$	172000.753(70)	27	$30_{4,27}-29_{4,26}$	343772.872(50)	−75
$15_{0,15}-14_{0,14}$	172001.112(70)	1	$30_{2,29}-29_{2,28}$	343845.881(50)	−5
$15_{2,13}-14_{2,12}$	172021.824(70)	37	$30_{3,28}-29_{3,27}$	343848.084(100)	4
$15_{1,14}-14_{1,13}$	172910.366(70)	29	$30_{3,27}-29_{3,26}$	343849.488(50)	−56
$20_{1,20}-19_{1,19}$	228124.750(50)	25	$30_{2,28}-29_{2,27}$	344014.301(50)	2
$20_{6,14}-19_{6,13}$	229106.527(50)	−35	$30_{1,29}-29_{1,28}$	345650.349(50)	9
$20_{6,15}-19_{6,14}$	229106.527(50)	−35			

Notes.
[a] Estimated experimental 1σ uncertainties in parentheses.
[b] For lines with hfs less than the experimental uncertainty, C is the intensity weighted average of the three strongest hyperfine components.

3. DISCUSSION

Thiocyanic acid was recently detected in Sgr B2 on the basis of the work here, and there is possible evidence of HSCN in published spectra of cold dark clouds. In Sgr B2, five consecutive $K_a = 0$ transitions were observed in the three millimeter-wave band (Halfen et al. 2009). The intensities, linewidths, and LSR velocities of HSCN and HNCS are comparable; the emission is cospatial and extended; and the column density of HSCN is only three times lower than that of the ground-state isomer

Table 3
Spectroscopic Constants of HSCN and DSCN (in MHz)

Constant	HSCN		DSCN	
	Laboratory	Theoretical[a]	Laboratory[b]	Theoretical[a]
A	289737(64)	285588	151350 (478)	149770
B	5794.71368(20)	5774.1	5705.09910(29)	5701.6
C	5674.93940(20)	5659.6	5489.24957(27)	5492.5
D_{JK}	0.15153(11)		0.14152(34)	
$10^3 D_J$	1.66557(21)		1.560(20)	
$10^6 d_1$	−35.91(21)			
$10^6 d_2$	−5.17(31)			
$10^6 H_{JK}$	0.518(26)			
$10^6 H_{KJ}$	−170.3(86)			
$10^6 L_{KKJ}$	−4.46(16)			
χ_{aa}(N)[c]	−4.0477(15)	−4.50	−4.0530(11)	−4.50
χ_{bb}(N)[c]	2.8271(18)	3.22	2.8292(18)	3.22
χ_{aa}(D)[c]			−0.0821(32)	−0.0549
χ_{bb}(D)[c]			0.1445(26)	0.141
Dipole moments (D):				
μ_a		3.46		3.46
μ_b		1.09		1.09

Notes.
[a] Rotational constants and dipole moments calculated at the B3LYP level of theory with a 6-311+G(d) basis (Durig et al. 2006); nitrogen quadrupole coupling constants (χ_{aa} and χ_{bb}) calculated with an aug-cc-pVTZ basis by us.
[b] Spectroscopic constants derived from seven transitions in the centimeter-wave band.
[c] The third quadrupole constant (χ_{cc}) was constrained, where $\chi_{cc} = -(\chi_{aa} + \chi_{bb})$.

HNCS. In TMC-1, two unidentified lines closely coincide in frequency with those of HSCN. Marcelino et al (2009) observed a line with the IRAM 30 m telescope (91750.68 ± 0.03 MHz) that we have assigned to the $8_{0,8}$–$7_{0,7}$ transition of HSCN (91750.630 ± 0.027 MHz). This line is most intense in TMC-1, but it was also observed in L1544 and B1, suggesting that HSCN may be present in many other dark clouds. A second unidentified line, whose frequency (45877.746 MHz, uncertainty ⩾ 20 kHz) is in good agreement with that of the $4_{0,4}$–$3_{0,3}$ transition (44877.800 ± 0.015 MHz), was observed in a wide band spectral line survey of TMC-1 with the Nobeyama 45 m Telescope (Kaifu et al. 2004). Unresolved hyperfine structure would account for the somewhat greater width (0.80 km s^{-1}) of the astronomical line at 44.9 GHz. A column density of HSCN in TMC-1 of (2–4) × 10^{11} cm^{-2} was estimated from these two lines, on the assumption that the rotational temperature is 6 K. HNCS was not observed in TMC-1 by Kaifu et al. (2004), implying that the HSCN/HNCS ratio of ⩾25% may be similar to that in Sgr B2.

Now that the astronomically most important rotational transitions have been measured in the laboratory, and HSCN has been identified in at least one astronomical source, observations in other galactic sources should follow. Measurements of the HSCN/HNCS ratio in sources with different physical and chemical environments may clarify how isomers are formed in the interstellar gas. Studies of HNC and HCN have shown that the abundance ratio of these two isomers is much greater in cold dark clouds than in sources with much higher kinetic temperatures (Hirota et al. 1998). If the identification of HSCN in dark clouds is confirmed, it would allow comparison of the HSCN/HNCS ratio with that in warm sources and possibly in hot cores if both isomers are detected.

Table 4
Effective Constants for the $K_a = 0$ and 1 Transitions of HSCN

K_a	E/k (K)	Effective Constants (in MHz)		
		B	$10^3 \times D$	$10^9 \times H$
0	0.0	5734.82973(27)	3.2452(13)	5.8(11)
1L	14.2	5704.73444(16)	2.0239(7)	5.8(6)
1U	14.2	5764.62154(13)	2.0955(6)	−4.4(5)

Notes. Effective constants derived from the least-squares fit to frequencies calculated with the constants in Table 3 neglecting hfs. Lines of astronomical interest can be calculated with the standard expression

$$\nu = 2BJ - 4DJ^3 + 2HJ^3(3J^2 + 1),$$

where J refers to the upper rotational level. The formal uncertainties in the calculated frequencies are ⩽0.2 km s^{-1} for transitions between 68 and 400 GHz.

Detection of the more abundant rare isotopic species would yield a precise molecular structure. Because lines of HSCN are very intense in our FTM spectrometer, it should be feasible to detect the rare isotopic species either in natural abundance or with isotopically enriched samples.

The present laboratory spectroscopy should be extended to higher frequencies in anticipation of observations of HSCN in the submillimeter-wave and THz bands. By analogy with the extensive work on HNCS (see Niedenhoff et al. 1997, and references therein), a full investigation of quasilinear HSCN may require measuring *b*-type transitions, pure rotational transitions in the low-lying vibrational states, and rotationally resolved IR spectra in the bending states.

This work is supported by NSF grant CHE-0701204 and NASA grant NNX08AE05G.

REFERENCES

Beard, C. I., & Dailey, B. P. 1950, J. Chem. Phys., 18, 1437
Brünken, S., Belloche, A., Martín, S., Verheyen, L., & Menten, K. M. 2009a, A&A, in press
Brünken, S., Gottlieb, C. A., McCarthy, M. C., & Thaddeus, P. 2009b, ApJ, 697, 880
Durig, J. R., Zheng, C., & Deeb, H. 2006, J. Mol. Struct., 784, 78
Frerking, M. A., Linke, R. A., & Thaddeus, P. 1979, ApJ, 234, L143
Gottlieb, C. A., Myers, P. C., & Thaddeus, P. 2003, ApJ, 588, 655
Halfen, D. T., Ziurys, L. M., Brünken, S., Gottlieb, C. A., McCarthy, M. C., & Thaddeus, P. 2009, ApJ, 702, L124
Hatchell, J., Thompson, M. A., Millar, T. J., & MacDonald, G. H. 1998, A&A, 338, 713
Hirota, T., Yamamoto, S., Mikami, H., & Ohishi, M. 1998, ApJ, 503, 721
Kaifu, N., et al. 2004, PASJ, 56, 69
Kewley, R., Sastry, K. V. L. N., & Winnewisser, M. 1963, J. Mol. Spectrosc., 10, 418
Marcelino, N., Cernicharo, P., Tercero, B., & Roueff, E. 2009, ApJ, 690, L27
McCarthy, M. C., Chen, W., Travers, M. J., & Thaddeus, P. 2000, ApJS, 129, 611
Müller, H. S. P., & Brünken, S. 2005, J. Mol. Spectrosc., 232, 213
Niedenhoff, M., Winnewisser, G., Yamada, K. M. T., & Belov, S. P. 1995, J. Mol. Spectrosc., 169, 224
Niedenhoff, M., Yamada, K. M. T., & Winnewisser, G. 1997, J. Mol. Spectrosc., 183, 176
Rodler, M., Jans-Bürli, S., & Bauder, A. 1987, Chem. Phys. Lett., 142, 10
Saito, S., Kawaguchi, K., Yamamoto, S., Ohishi, M., Suzuki, H., & Kaifu, N. 1987, ApJ, 317, L115

Schuurman, M. S., Muir, S. R., Allen, W. D., & Schaefer, H. F. 2004, J. Chem. Phys., 120, 11586
Wakelam, V., Caselli, P., Ceccarelli, C., Herbst, E., & Castets, A. 2004, A&A, 422, 159
Wierzejewska, M., & Mielke, Z. 2001, Chem. Phys. Lett., 349, 227
Wierzejewska, M., & Moc, J. 2003, J. Phys. Chem. A, 107, 11209
Yamada, K., Winnewisser, M., Winnewisser, G., Szalanski, L. B., & Gerry, M. C. L. 1979, J. Mol. Spectrosc., 78, 189
Yamada, K., Winnewisser, M., Winnewisser, G., Szalanski, L. B., & Gerry, M. C. L. 1980, J. Mol. Spectrosc., 79, 295
Yamamoto, S., Saito, S., Kawaguchi, K., Kaifu, N., & Suzuki, H. 1987, ApJ, 317, L119